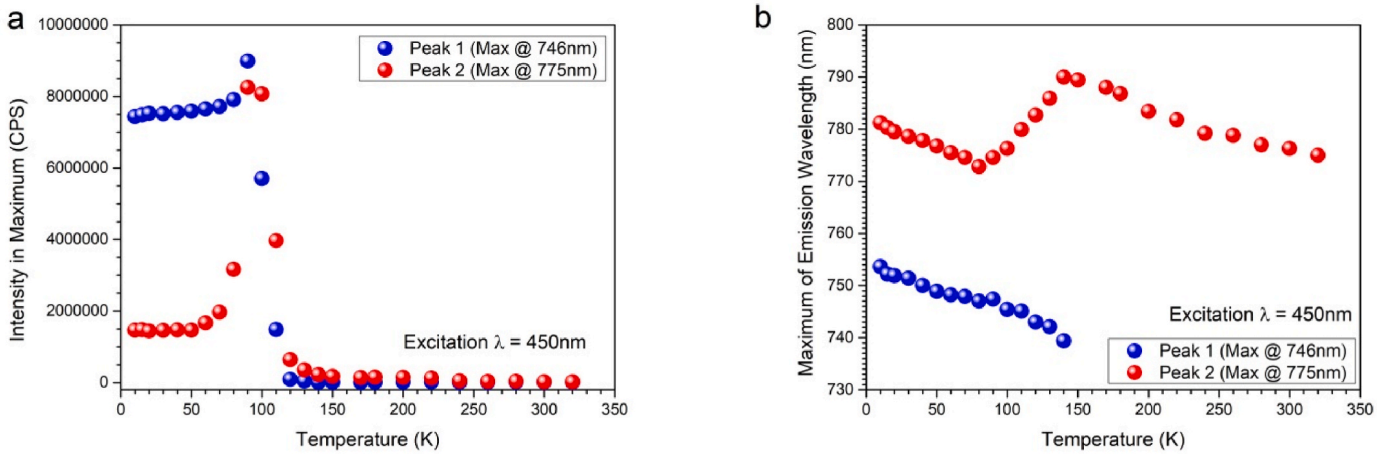


Fig. 12. Dependence of the maximum intensity for $MAPbI_3$ PL spectra as a function of the temperature (a) and maximum PL wavelength (b).

series with a current meter (I-METER) and in parallel with a voltage meter (V-METER). Voltage (V-limit) and current (I-limit) protection systems limit the voltage or current to the programmed value. When measuring the resistance of the layers, the SMU acts as a voltage source supplying the tested thin perovskite film and at the same time the current flowing in the circuit is measured.

The influence of tested perovskite layer's illumination is visible in the current-voltage characteristics (Fig. 13a–d). In the case of resistance measurements of thin perovskite layers, the sample was placed in a Janis CCR-CTI cryostat, which enabled measurements in the broad range from liquid helium to room temperature. The LCS-100 sunlight simulator (Oriel) was used to test the sample in lighting conditions. The LCS-100 sunlight simulator is intended for research requiring the operation of a certified system in a small lighting area. This simulator allows for uniform illumination of surfaces measuring 1.5 × 1.5 inches (38 × 38 mm) and meets ABB Class requirements under ASTM and IEC standards.

BK7 glass with two strips of copper contacts was used as a substrate for the layers subjected to resistance and temperature dependence tests. The contacts were made in the PVD process and are 150 nm thick, 1.5 mm wide, and 5 mm apart. Samples in the form of thin layers with a

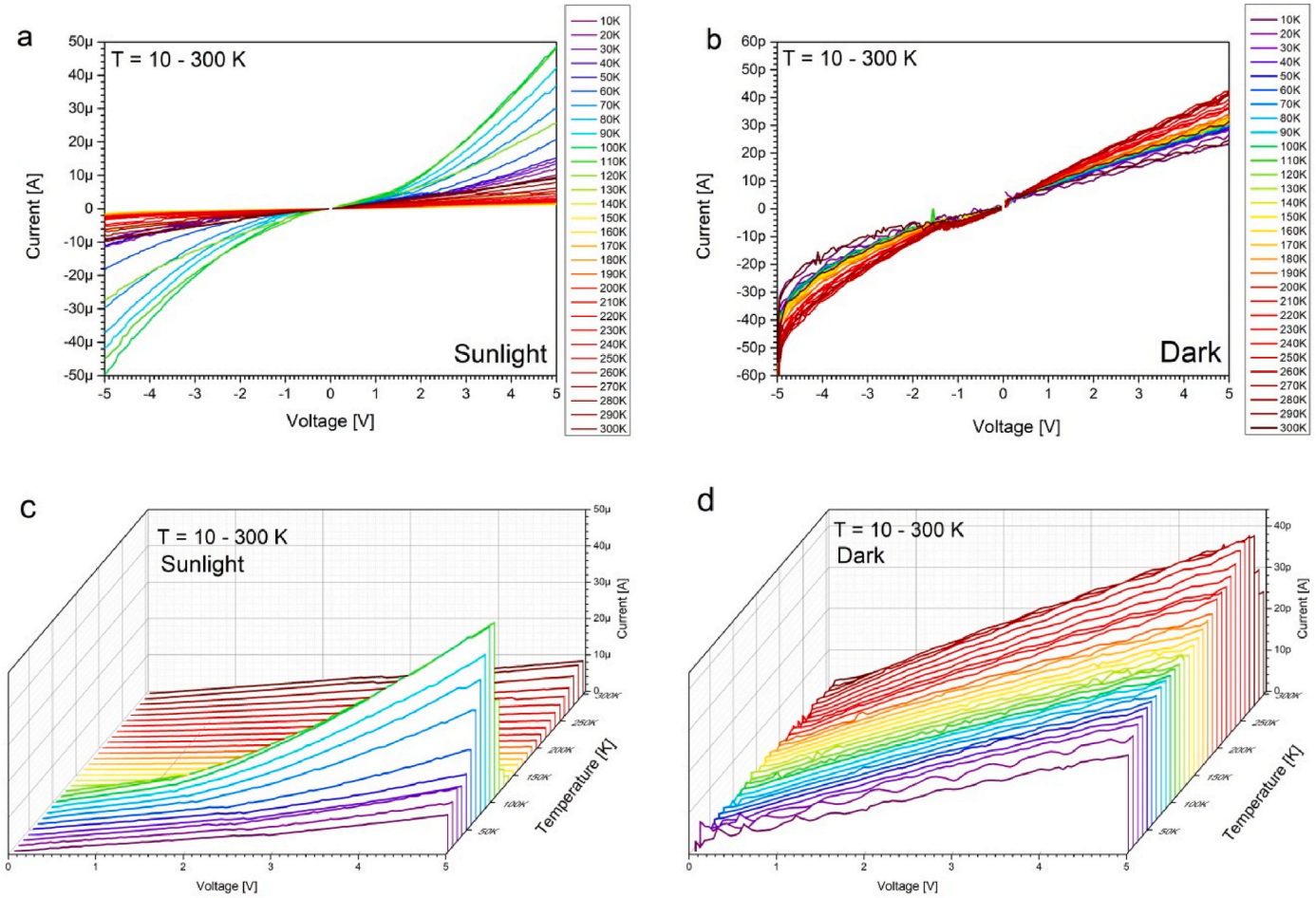


Fig. 13. Temperature dependences of the resistance of the $MAPbI_3$ layer under artificial sunlight (a, c) and darkness (b, d).

thickness of 300 nm were used to carry out resistance tests. Measurements in light and no light conditions were performed in one measurement for the same sample at each temperature. Experimental I–V characteristics allow us to notice significant differences in the values and behavior of resistance as a function of temperature for the tested thin layer.

In the case of tests performed in complete darkness, the intensity of currents flowing through the layer reached several dozen pico-amperes at several volts. The obtained characteristics were almost symmetrical concerning zero on the applied voltage scale, and the dependence of I on V was linear. As the temperature increased, the observed current flowing through the layer increased slightly. Using Ohm's law, the resistance of the thin film was calculated, and for no-light conditions, the value was in the order of several hundred giga-ohms and for 300 K it was about twice as small as for 10 K. It allows us to conclude that the $MAPbI_3$ perovskite thin film behaves like a semiconductor in the absence of light. The results obtained for measurements under layer illumination conditions are more complex. The I–V characteristics are still symmetrical towards zero, but the linear relationship between current and voltage is no longer maintained. It confirms the semiconductor nature of the layer. Additionally, the change in the values of the measured currents as a function of voltage (and, therefore, the layer resistance) is not monotonic. The division of the I–V characteristic into two parts is clearly visible. In the temperature range from 10 K to 120 K, the resistance values ranged from several dozen to several hundred kilo-ohms, and a constant monotonic decrease in resistance was observed with an increase in temperature. In the range of 120–140 K, there was a sudden change in resistance by approximately an order of magnitude. Again, from a temperature of 150 K, a monotonic decrease in resistance was observed with an increase in temperature.

Interestingly, the final resistance values for 10 K and 300 K were similar and amounted to about 500 kilo-ohms. Moreover, the difference in resistance in light and no light conditions was five orders of magnitude. Detailed characteristics of the resistance as a function of temperature for the layer under lighting and low-light conditions are presented in Fig. 14a–b.

5. Hybrid perovskite solar cells with photoactive $MAPbI_3$ thin film

Our research focused on several essential factors for the practical use of thin films of hybrid perovskites in solar cells. The first was a technique for manufacturing the entire solar cell structure in a high vacuum environment. We assumed that the whole structure of the cell, i.e., the electron transporting layer (ETM), the active perovskite layer, and the hole transporting layer (HTM), should be made during a three-stage deposition process to minimize the impact of the external environment on the composition and purity of the deposited layers. Transparent conductive and metallic contacts can be made in separate processes. The second was that each layer's material in the cell structure should have a sublimation temperature, enabling the deposition of the entire cell on both a glass substrate and PET foil. The third goal was to obtain solar cells with the same parameters (layer thickness, cell efficiency, etc.) and to ensure the repeatability of the process. The final goal was to achieve cell efficiency comparable to silicon solar cells currently available on the market.

Based on the above assumptions, we have developed a cell structure consisting of ITO - transparent conductive electrode, SnO_2 - electron transporting layer, $CH_3NH_3PbI_3$ hybrid perovskite - light-harvesting active layer, Spiro-MeOTAD - hole transporting layer, and gold - metallic contact. Fig. 15 shows a diagram of the energy levels of the materials constituting perovskite solar cells (a), the architecture of the tested cells (b), and a picture of studied perovskite solar cells with $CH_3NH_3PbI_3$ hybrid perovskite photoactive layer deposited by PVco-D and Spin-Coating techniques (c).

5.1. Optimization of a perovskite solar cell

The SCAPS-1D – one dimensional solar cell simulation program developed at the Department of Electronics and Information Systems (ELIS) of the University of Gent, Belgium, was used to optimize the perovskite solar cell architecture [46]. To carry out the optimization process, all necessary tests were previously performed for the individual layers of the cell. Since all layers were made in the PVD process (classical method and co-deposition), physical constants were used for optimization based on the research described in the previous sections, for both perovskite layers and those transporting holes and electrons.

The simulated results indicate that hole and electron transport layers with a thickness of less than 100 nm do not significantly affect the efficiency of the developed cell. In contrast, the thickness of the perovskite layer (Fig. 16c) and the selection of appropriate metallic contacts (Fig. 16b) are of great importance. Fig. 16b shows that the potential replacement of gold contacts by other metals except platinum) will lead to a reduction in solar cell efficiency. Unfortunately, cheaper alternative metallic materials were ineffective in the tested cell design.

In the case of $MAPbI_3$ perovskite layers, simulations showed the optimal layer thickness, which should be approximately 500–600 nm in the proposed structure. Interestingly, using thinner layers led to decreased cell efficiency due to the porosity of the perovskite structure and diffusion processes. Fig. 17 shows the current-voltage characteristics of the proposed $MAPbI_3$ perovskite solar cell as a function of the $MAPbI_3$ perovskite layer thickness under one solar illumination.

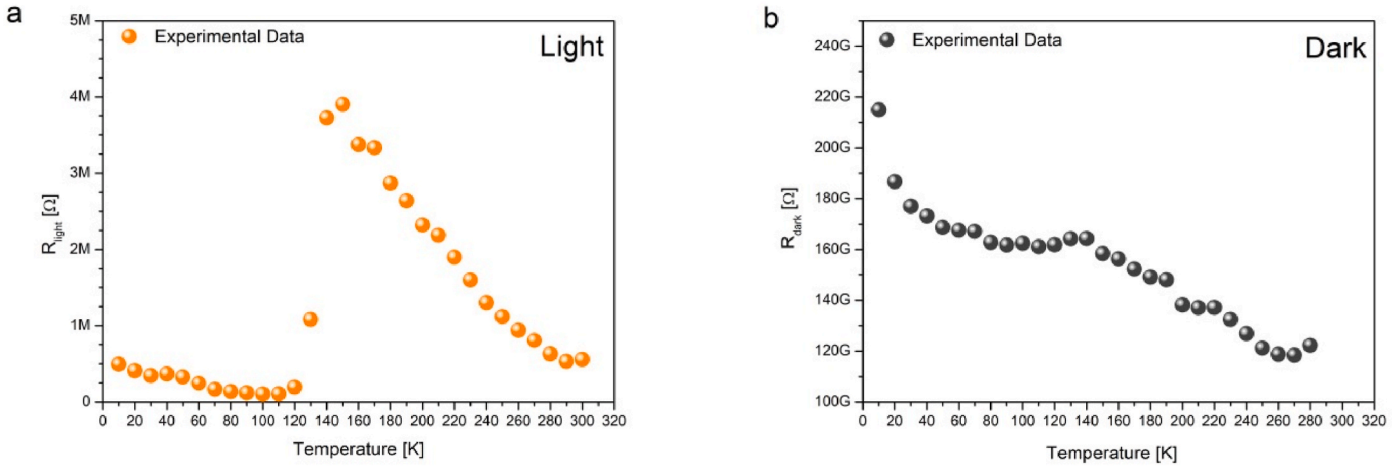


Fig. 14. Resistance of the $MAPbI_3$ layer as a function of the temperature: in light (a) and dark (b).

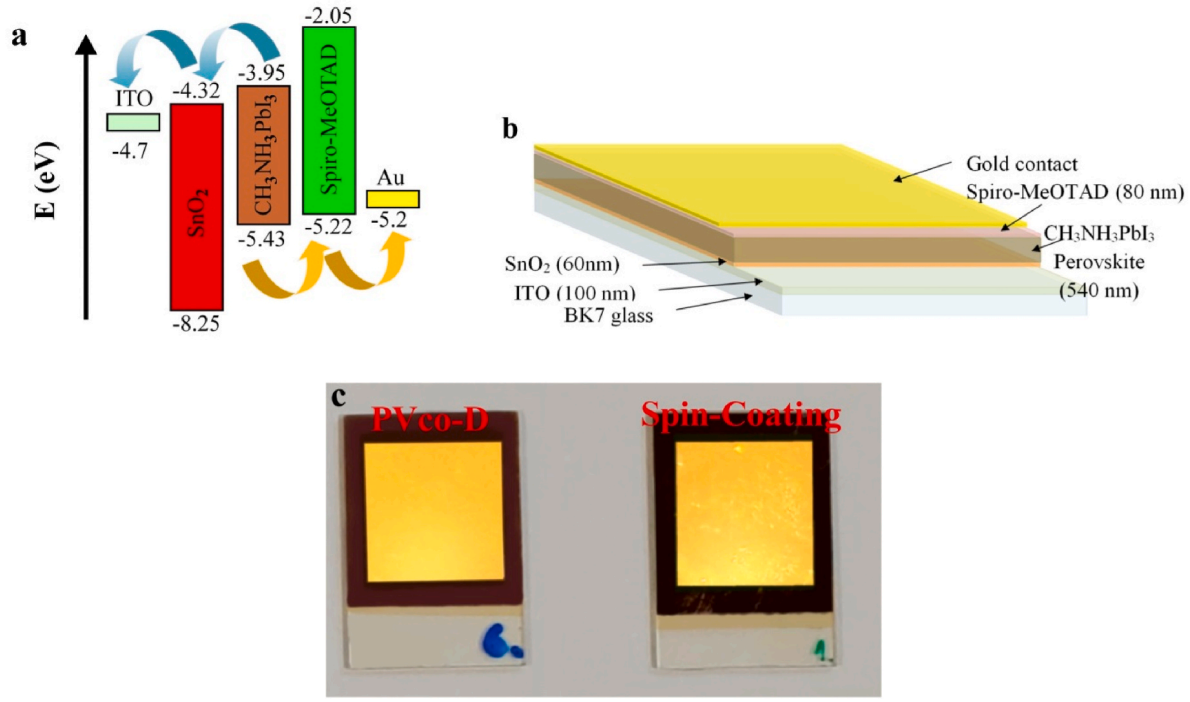


Fig. 15. Energy level diagram (a), architecture of studied perovskite solar cells (b) and picture of studied perovskite solar cells with $CH_3NH_3PbI_3$ hybrid perovskite photoactive layer deposited by PVco-D and Spin-Coating techniques (c).

5.2. Perovskite solar cell - comparison of experimental studies and simulations

To compare the results obtained from simulations performed in the SCAPS-1D program, the structure of a complete solar cell presented in Fig. 15b was deposited. The surface of the produced cells had the shape of a rectangle with side dimensions of 2.5 by 3 cm. The current-voltage characteristics of perovskite solar cells were measured using the measurement system shown in Fig. 18.

The experimental setup included the KEITHLEY 4200-scs measuring system, equipped with three SMU and LCS-100 sunlight simulator (Oriel). The SMU can work as a voltage or current source (depending on the selected function) and is connected in series with a current meter (I-METER) and in parallel with a voltage meter (V-METER). A pair of FORCE wires were used in the measurements, while the SENSE wires were shorted to the ground. Cell measurements were made under atmospheric pressure and room temperature, and the measurement probes' positions were manually adjusted using micromanipulators. The LCS-100 sunlight simulator was used to test the sample in lighting conditions. For standard solar cell measurements, the spectrum was standardized to the AM1.5 spectrum. The influence of illumination on the tested perovskite solar cell is visible in the experimental current-voltage characteristic presented in Fig. 19. The tested cell showed a significant response to illumination with simulated sunlight. The obtained short-circuit current J_{SC} and open-circuit voltage V_{OC} were 23,59 mA/cm^2 and 1.07 V, respectively. The obtained efficiency at room temperature was equal to ca.18.5 %. It is worth noting that the tested cell also showed a low efficiency of 0.4 % in dark conditions.

A comparison of the characteristics of current and power densities as a function of voltage measured in the experiment with the result of the structure optimized in the SCAPS-1D program is shown in Fig. 20a–b.

A comparison of the parameter values for perovskite solar cells made in the vacuum sublimation process and the simulation of its operation in the SCAPS-1D program shows their high compliance. Simulations in the SCAPS-1D program were extremely helpful in designing the structure of a perovskite cell and significantly improved the work on creating an optimal structure using the classic and co-deposition PVD processes.

Based on the high compliance of simulations for a cell operating at room temperature and using the physical parameters obtained for thin layers constituting the cell, simulations of its operation in the temperature range from 10 K to 300 K were carried out. The simulations were performed in the SCAPS-1D program, and the simulations used changes in parameters (previously determined for all layers composing a solar cell) such as changes in the crystal phase, changes in energy gap, changes in resistance, hole and electron concentration, structure defects, changes in radiative recombination, etc.

These simulations allowed several results to be obtained regarding the potential operation of the solar cell in conditions of reduced temperature and pressure, which is attractive due to the possible use of perovskite cells in space. The results are presented in Fig. 21a–c.

The analysis of the obtained results leads to several interesting conclusions. Firstly, at the temperature corresponding to the transition from the orthorhombic to the tetragonal phase, there will be a sudden change in the values of parameters such as short-circuit current J_{SC} open-circuit voltage V_{OC}, current and voltage at the point of maximum power, J_{MPP} and V_{MPP}, respectively. However, changes in the fill factor FF and efficiency will be mild. The result of the performance simulation in the tested temperature range is significant for application purposes. The cell showed similar efficiency values throughout the simulated temperature range: 18.2–18.7 %. Slight disturbances in cell efficiency occurred in the temperature range corresponding to the change in the crystallographic phase. Nevertheless, this disturbance will not significantly affect the continuity of the cell's operation because it leads to a slight increase in its efficiency. It makes the cell with the proposed architecture fabricated using vacuum co-deposition (PVco-D) techniques up-and-coming for applications in space.

5.3. Perovskite solar cell parameters - comparison of photoactive layer $CH_3NH_3PbI_3$ deposition techniques

To compare the impact of the hybrid perovskite layer deposition technique on the basic parameters of the perovskite solar cell, two similar cells were prepared, differing in the method the $CH_3NH_3PbI_3$ layer was made. In these cells, the hole (HTM - SpiroMeOTAD) and

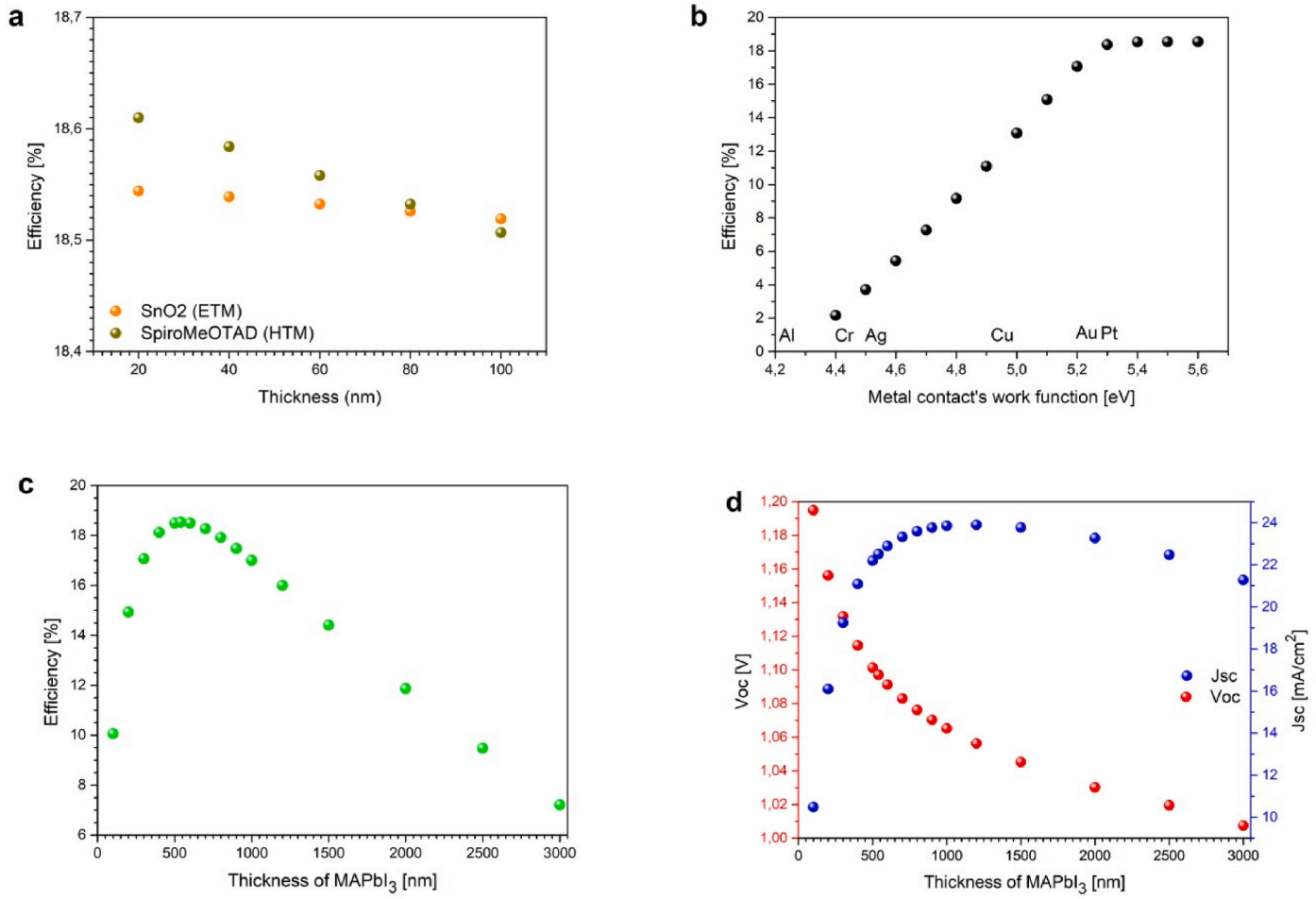


Fig. 16. Cell structure optimization diagrams: efficiency as a function of ETM and HTM (a), efficiency as a function of metal contact's work function (b), efficiency as a function of $MAPbI_3$ layer thickness (c), dependences of V_{OC} and J_{SC} on $MAPbI_3$ layer thickness (d).

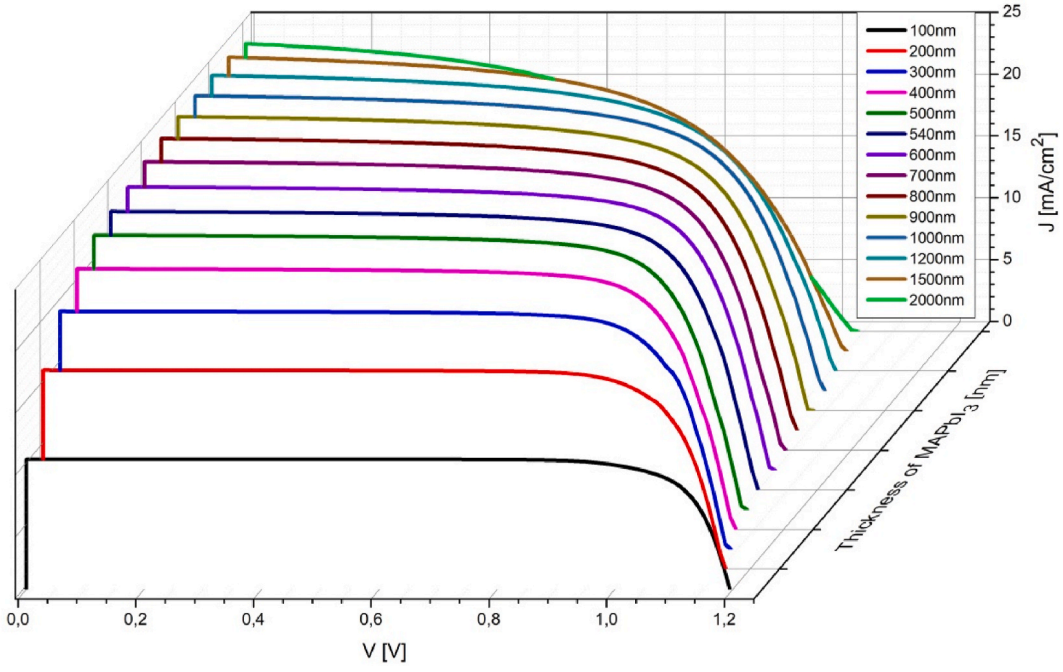


Fig. 17. I–V characteristics of the PTFCS as a function of the $MAPbI_3$ perovskite layer thickness.

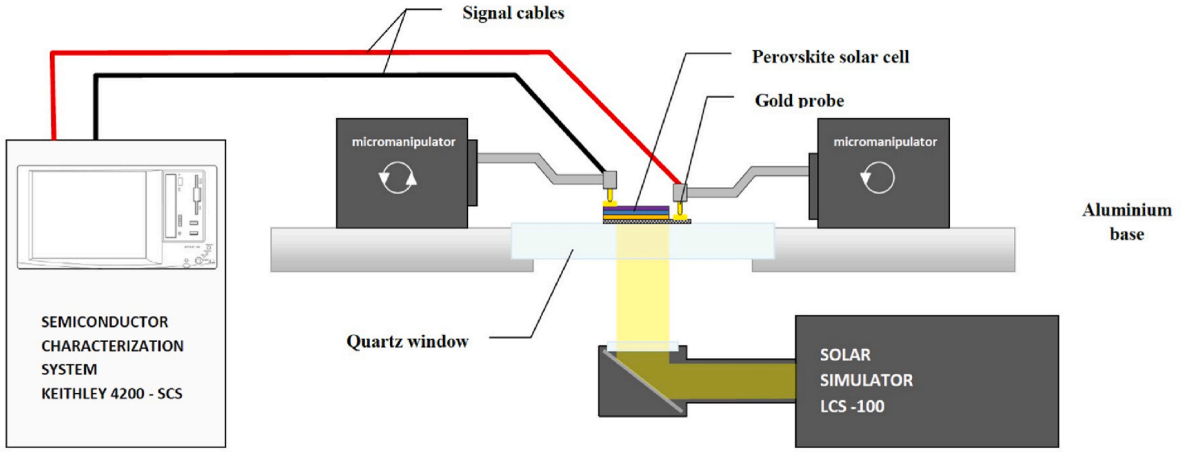


Fig. 18. Diagram of the measurement system for testing the electrical properties of perovskite solar cells.

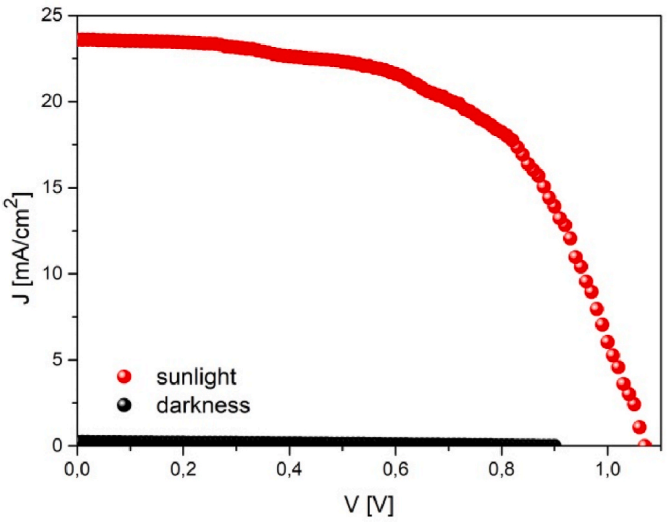


Fig. 19. Experimental current-voltage characteristics of the tested PTFSC in dark and light illumination conditions.

electron (ETM – SnO_2) transport layers, as well as the transparent conducting (ITO) and gold (Au) contacts, were made during the same processes. However, the hybrid perovskite layer was made using two deposition techniques: PVco-D, discussed in this article, and spin-coating, commonly used to produce perovskite solar cells. Methylammonium triiodoplumbate (II) precursor solution 40 wt % in DMF (Sigma-Aldrich) was used to obtain a spin-coating layer. The complete spin-coating process was carried out in the surrounding atmosphere and under normal pressure conditions by heating the $CH_3NH_3PbI_3$ film to a temperature of 110 °C until it crystallized. Unfortunately, the spin-coating process, which uses the increased temperature necessary for crystallization, leads to significant porosity of the layer. Porosity, in turn, made it impossible to obtain a uniform layer on the entire cell surface. Therefore, for the layer created using the spin-coating technique, we can only use the average layer thickness, approximately 600 nm (the thickness measured in various places of the layer ranged from 500 to 650 nm). The obtained spin-coating layer also differed by several percent in physical parameters such as energy gap (1.62eV), refractive index (2.4), and phase transition temperature range (130–160 K).

The use of two techniques allowed for a comparison of the impact of the perovskite layer production technique on the basic parameters of the solar cell. The current-voltage characteristics of solar cells immediately after their manufacture and six months later are presented in Fig. 22 a-d.

The analysis of current and power characteristics as a function of voltage leads to several fundamental conclusions. Firstly, regardless of the technique used to make the perovskite photoactive layer, both cells operated for six months, although their basic parameters significantly differed. Secondly, the shape of the curves describing cells with a perovskite photoactive layer depends on its production technique. The shape of the curves with the layer made using the PVco-D technique is typical for solar cells. However, for the layer made using the spin-

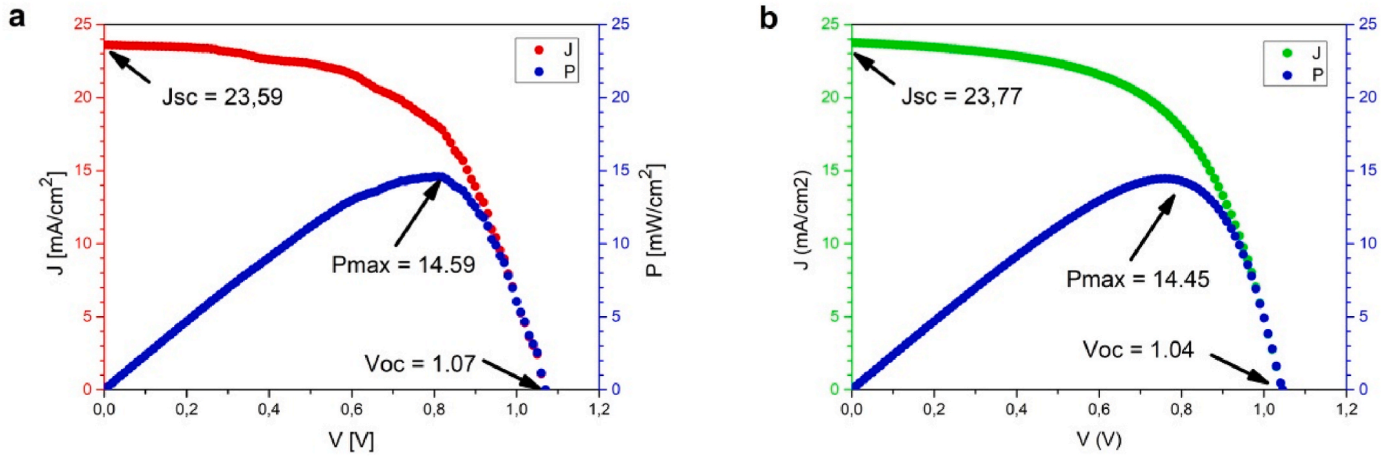


Fig. 20. Basic characteristics of the cell: measured current and power density as a function of voltage (a), simulated in the SCAPS-1D program (b).

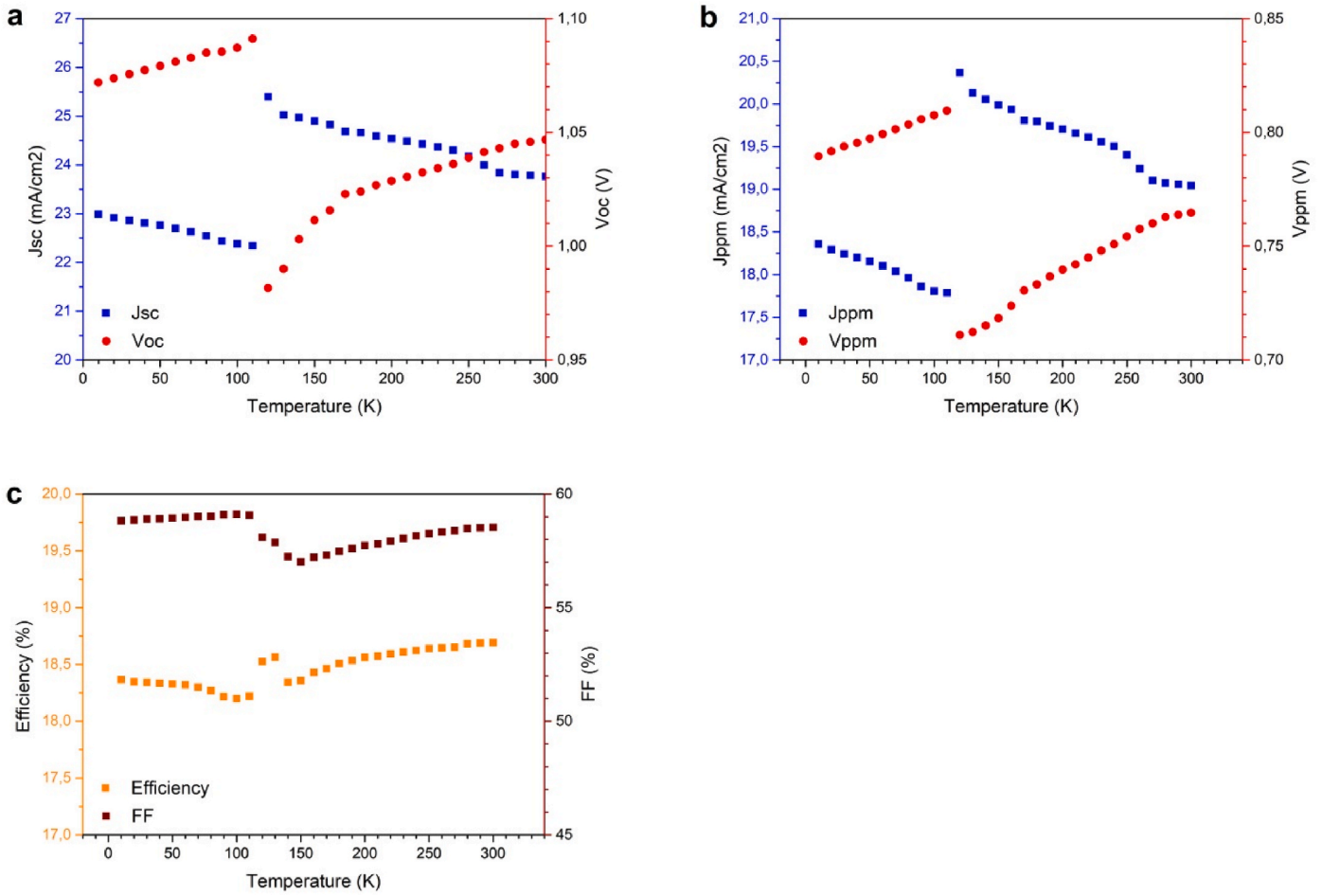


Fig. 21. Basic characteristics of the PTFSC as a function of the work's temperature simulated in the SCAPS-1D program: J_{SC} and V_{OC} (a), J_{MPP} and V_{MPP} (b), and FF and efficiency (c).

coating method, a clear "straightening" of the dependence of the current flowing through the cell as a function of voltage was observed (FF decreased). After six months of operation, the current-voltage characteristic was close to a straight line, and the power-voltage dependence was almost symmetrical. It proves that the bands of the HTM and ETM layers are less adjusted to the energy levels of the spin-coated perovskite layer. Thirdly, solar cells with a photoactive perovskite layer deposited by the PVco-D technique showed a higher short-circuit current, a higher open-circuit voltage, and almost three times higher maximum power. After six months, the value of the open circuit voltage remained unchanged, and the value of the short-circuit current decreased slightly, causing a change in the maximum power. These differences were much more significant in the case of cells with a spin-coating layer. The observed behavior of cells over time indicates an increase in their internal resistance, which is more critical for cells made with perovskite spin-coating films.

5.4. Stability of the perovskite solar cells

Seven solar cells were made to investigate the temporal stability of the basic parameters of perovskite solar cells, such as short-circuit current J_{SC}, open-circuit voltage V_{OC}, maximum power P_{max}, and fill factor FF. Six were made using the PVco-D process to deposit a perovskite absorption layer. For comparison purposes, one cell was also made with an absorption layer deposited by the spin-coating technique. Fig. 23a–d and Table 2 show the dependencies of the basic parameters of the cells measured immediately after their fabrication, one month later, and after 3 and 6 months.

The analysis of the experimental data collected in the graphs indicates that after six months, all tested cells still generate a potential difference between the electrodes (ITO and Au) under the influence of sunlight, and the values of the essential cells' parameters depend on the technique used to create the perovskite absorption layer. Measurements of current-voltage characteristics indicate that cells with a perovskite layer made in the PVco-D process are much more stable over six months. For all six cells fabricated in the same PVco-D process, the open-circuit voltage value practically did not change over the entire period (changes at the level of 2 % of the value). However, a more significant decrease in the short-circuit current value was observed (changes of approximately 17 % of the value), which ultimately reduced the maximum power generated by the cells by approximately 20 % and the fill factor by approximately 10 %. For comparison, the open-circuit voltage value for a cell with a spin-coated absorption layer was 10 % lower and dropped by over 25 % over the same six-month period. The initial value of the short-circuit current was 20 % lower and decreased by 15 % compared to the initial value. The maximum power was three times lower than for PVco-D, and its decrease after six months was more significant and amounted to over 60 % of the initial value. The initial value of the fill factor was 40 % lower compared to the cell with the PVco-D layer, and its decrease was about 20 % reduction.

The obtained results indicate that using a photoactive layer made by the PVco-D technique in a perovskite solar cell not only increases the efficiency of the cell by several percent but also significantly improves its temporal stability. The observed decrease in the short-circuit current value with an unchanged open circuit voltage value under Ohm's law indicates an increase in the cell's internal resistance caused by the

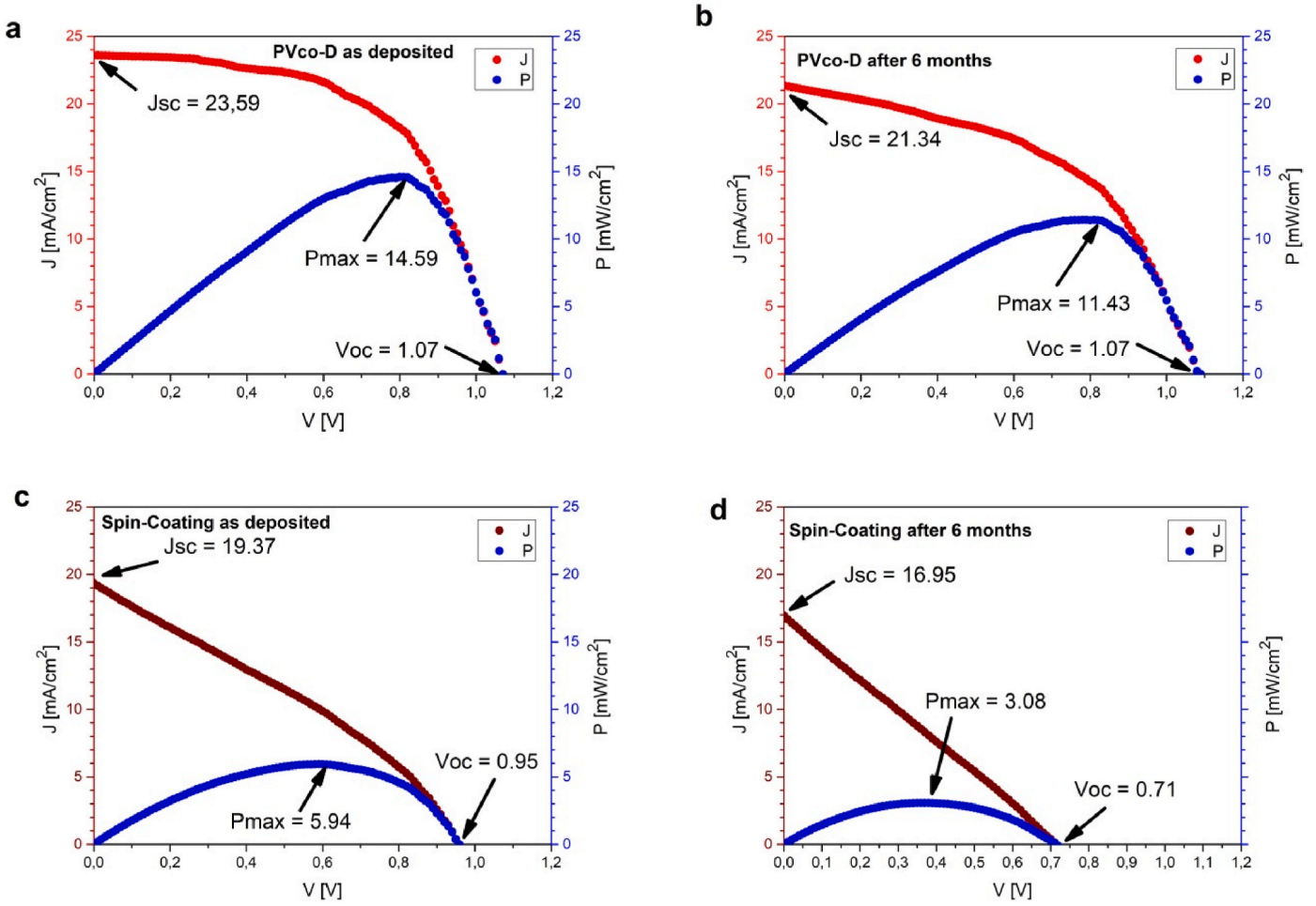


Fig. 22. The current - voltage characteristics of solar cells with $CH_3NH_3PbI_3$ active film deposited by different technique: PVco-D as deposited (a), PVco-D six months later (b), spin-coating as deposited (c), spin-coating six months later (d).

degradation of the internal structure of the perovskite absorption layer. As is commonly known, perovskite layers are highly hygroscopic, and their degradation occurs due to the adsorption of water and water vapor molecules contained in the surrounding environment. Due to the much higher density and packing of particles in the perovskite PVco-D layer, degradation is limited to a small area. Moreover, compared to a porous layer made in the spin-coating process, this degradation is significantly smaller, and the cells retain parameters similar to the initial ones for much longer. It makes the PVco-D technique proposed in this work extremely promising for producing perovskite cells. Considering the practically zero water content in space, it can be assumed that the perovskite solar cell will operate much longer in such conditions [47]. Experimental studies of the temperature dependences of the layers constituting solar cells presented in this work indicate that low temperature will not significantly affect the efficiency of the cells.

6. Conclusions

In summary, we have described an innovative process for obtaining hybrid perovskites in thin layers and complete solar cell structures using these layers to accumulate sunlight and convert it into electricity. The developed PVco-D process using two independent thermal sources in the vacuum sublimation process allows for obtaining thin layers of hybrid and inorganic perovskites with various chemical compositions and high uniformity over a large surface. Moreover, such a process can be repeated many times while maintaining identical, and the produced layers and perovskite solar cells have similar parameters. This work presents experimental data, such as the refractive index, absorption and extinction coefficients, complex dielectric constant, and optical energy gap, necessary to simulate the operation of solar cells. The PVco-D process and the complete solar cell structures were subjected to a detailed analysis of their structural, optical, and electrical properties in a wide temperature range from 10 K to 320 K. The results of testing the optical parameters of MAPbI3 layers obtained in the proposed vacuum process (i.e., optical energy gap, absorption band edge, radiative recombination) and electrical parameters (resistance) show abrupt changes in values in the temperature range responsible for the phase transition from the orthorhombic to the tetragonal phase.

Moreover, it was not possible to determine one value of the phase transition temperature for the examined layers, but only the interval in which both phases coexisted. It resulted from a much greater layer order and density than those obtained in processes using precursor solutions. It, in turn, increased the absorption capacity of the layers and reduced its resistance by five orders of magnitude when illuminated with sunlight. Using such perovskite layers allowed the development and fabrication of a complete solar cell structure with a thickness of less than 1 μm, i.e., less than the thickness of a human hair. Optimization of the cell structure performed in the SCAPS-1D program allowed the creation of a thin-film perovskite solar cell with an efficiency of approximately 18.5 % in a wide temperature range from 10 K to 320 K, which is very promising in mass production.

Research on the repeatability of the production process and the stability of fabricated cells indicates a significant improvement in the basic parameters of the cells compared to the commonly used spin-

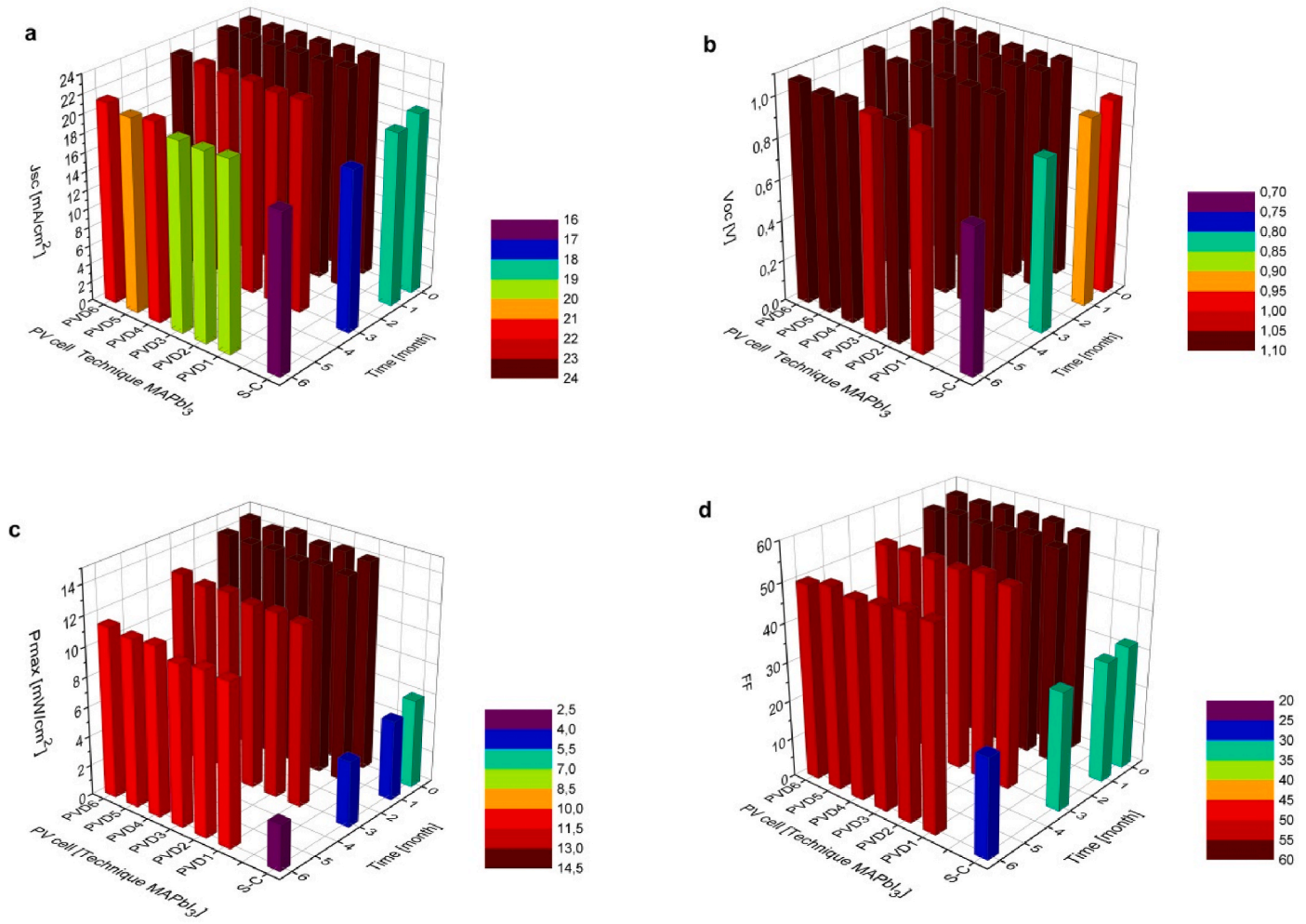


Fig. 23. Stability of the perovskite solar cells' basic parameters: J_{SC} (a), V_{OC} (b), P_{max} (c), FF (d).

Table 2
Main parameters of perovskite solar cells and their aging within six months of operation.

Solar Cells Parameters		Type of Perovskite Active Layer						
		Spin –Coating	Physical Vapor co-Deposition (PVco- D)					
		(S–C)	PVD1	PVD2	PVD3	PVD4	PVD5	PVD6
V_{OC} [V]	as deposited	0.95	1.06	1.05	1.05	1.07	1.06	1.07
	1 month	0.92	1.06	1.05	1.05	1.07	1.05	1.07
	3 month	0.84	1.05	1.05	1.05	1.07	1.05	1.07
	6 month	0.71	1.04	1.05	1.04	1.06	1.05	1.07
J_{SC} [mA/cm^2]	as deposited	19.37	23.52	23.55	23.49	23.51	23.55	23.59
	1 month	18.57	23.47	23.43	23.45	23.44	23.49	23.54
	3 month	17.23	22.43	22.31	22.65	22.58	22.76	22.93
	6 month	16.95	20.16	20.05	20.15	21.15	20.69	21.34
P_{max}	as deposited	5.94	14.08	14.26	14.12	14.46	14.22	14.49
[mW/cm^2]	1 month	5.37	13.82	13.98	13.78	14.01	13.94	14.09
	3 month	4.43	12.15	12.33	12.28	12.59	12.47	12.75
	6 month	3.08	10.87	10.98	10.76	11.35	11.22	11.43
FF [%]	as deposited	32.28	56.48	57.69	57.25	57.48	56.94	57.41
	1 month	31.43	55.55	56.83	55.97	55.86	56.52	55.94
	3 month	30.61	51.59	52.63	51.63	52.11	52.18	51.97
	6 month	25.59	51.84	52.16	51.35	50.63	51.65	50.06

coating technique and a substantial slowdown in the degradation process. Therefore, it makes the cell with the proposed architecture fabricated using vacuum co-deposition (PVco-D) techniques up-and-coming for applications in space.

Currently, our laboratory is conducting research on optimizing cell devices and architecture to improve energy conversion efficiency further.

CRediT authorship contribution statement

Anna Zawadzka: Writing – review & editing, Writing – original draft, Supervision, Project administration, Funding acquisition, Formal

analysis, Data curation, Conceptualization. **Agnieszka Marjanowska:** Visualization, Methodology, Investigation. **Amina Laouid:** Investigation, Formal analysis, Conceptualization. **Krzysztof Wisniewski:** Validation, Investigation, Formal analysis. **Youssef El Kouari:** Writing – review & editing, Visualization, Methodology. **Youssef El Hani:** Investigation, Formal analysis, Data curation. **Przemysław Płóciennik:** Writing – review & editing, Visualization, Software, Methodology, Investigation, Formal analysis, Data curation.

Declaration of competing interest

The authors declare that they have no known competing financial interests or personal relationships that could have appeared to influence the work reported in this paper.

Data availability

Data will be made available on request.

Acknowledgements

This research has been financed from the funds of the Polish National Science Centre (grant no. 2017/25/B/ST7/02124). The films used in this paper were obtained using Interdisciplinary Centre for Modern Technologies facilities, NCU, Torun, Poland. The research was carried out as part of the IDUB project - emerging research fields: “Material Science and Technology”.

References

[1] W.S. Yang, et al., High-performance photovoltaic perovskite layers fabricated through intramolecular exchange, Science 348 (2015) 1234–1237, https://doi.org/10.1126/science.aaa9272.
[2] J.-P. Correa-Baena, et al., Promises and challenges of perovskite solar cells, Science 358 (2017) 739–744, https://doi.org/10.1126/science.aam632.
[3] C. Roldán-Carmona, et al., High efficiency methylammonium lead triiodide perovskite solar cells: the relevance of non-stoichiometric precursors, Energy Environ. Sci. 8 (2015) 3550–3556, https://doi.org/10.1039/C5EE02555A.
[4] A.M.A. Leguy, et al., The dynamics of methylammonium ions in hybrid organic–inorganic perovskite solar cells, Nat. Commun. 6 (2015) 7124, https://doi.org/10.1038/ncomms8124.
[5] R.E. Wasylishen, Osvald Knop, J.B. Macdonald, Cation rotation in methylammonium lead halides, Solid State Commun. 56 (7) (1985) 581–582, https://doi.org/10.1016/0038-1098(85)90959-7.
[6] A.M. Alamri, et al., Fully inkjet-printed photodetector using a graphene/perovskite/graphene heterostructure, IEEE Trans. Electron. Dev. 66 (2019) 2657–2661, https://doi.org/10.1109/TED.2019.2911715.
[7] S. Öz, et al., Zero-dimensional (CH_3NH_3)3Bi2I9 perovskite for optoelectronic applications, Chem. Phys. Lett. 647 (2016) 7–13, https://doi.org/10.1016/j.cplett.2016.01.041.
[8] M. Fievez, et al., Slot-die coated methylammonium-free perovskite solar cells with 18% efficiency, Sol. Energy Mater. Sol. Cell. 230 (2021) 111189, https://doi.org/10.1016/j.solmat.2021.111189.
[9] B.C. O'Regan, et al., Optoelectronic studies of methylammonium lead iodide perovskite solar cells with mesoporous TiO_2: separation of electronic and chemical charge storage, understanding two recombination lifetimes, and the evolution of band offsets during *J–V* hysteresis, Am. Chem. Soc. 137 (2015) 5087–5099, https://doi.org/10.1021/jacs.5b00761.
[10] S. Mirershadi, et al., Third order nonlinear optical properties of organometal halide perovskite by means of the Z-scan technique, Chem. Phys. Lett. 647 (2016) 7–13, https://doi.org/10.1016/j.cplett.2016.01.041.
[11] Ch Zhang, et al., Iodide and charge migration at defective surfaces of methylammonium lead triiodide perovskites: the role of hydrogen bonding, Appl. Surf. Sci. 604 (2022) 154501, https://doi.org/10.1016/j.apsusc.2022.154501.
[12] W.-C. Lai, et al., Conversion efficiency enhancement of methylammonium lead triiodide perovskite solar cells converted from thermally deposited lead iodide via thin methylammonium iodide interlayer, Org. Electron. 82 (2020) 105713, https://doi.org/10.1016/j.orgel.2020.105713.
[13] A. Kojima, et al., Organometal halide perovskites as visible-light sensitizers for photovoltaic cells, J. Am. Chem. Soc. 131 (2009) 6050–6051, https://doi.org/10.1021/ja809598r.
[14] A. Jaffe, et al., High-pressure single-crystal structures of 3D lead-halide hybrid perovskites and pressure effects on their electronic and optical properties, ACS Cent. Sci. 2 (4) (2016) 201–209, https://doi.org/10.1021/acscentsci.6b00055.
[15] Best Research-Cell Efficiencies" *(PDF)*, National Renewable Energy Laboratory, 2023-08-28. https://www.nrel.gov/pv/assets/pdfs/best-research-cell-efficiencies-rev220630.pdf.
[16] H. Min, et al., Perovskite solar cells with atomically coherent interlayers on SnO_2 electrodes, Nature 598 (7881) (2021) 444–450, https://doi.org/10.1038/s41586-021-03964-8.
[17] M. De Bastiani, et al., Efficient bifacial monolithic perovskite/silicon tandem solar cells via bandgap engineering, Nat. Energy 6 (2021) 167–175, https://doi.org/10.1038/s41560-020-00756-8.
[18] K.E. Koné, et al., Insight into the effect of halogen X in methylammonium lead halide (MAPbX3) spin-coated on zinc oxide film, Opt. Mater. 135 (2023) 113238, https://doi.org/10.1016/j.optmat.2022.113238.
[19] J. Marí-Guaita, et al., Stability improvement of methylammonium lead iodide perovskite thin films by bismuth doping, JOM 74 (2022) 3103–3110, https://doi.org/10.1007/s11837-022-05347-4.
[20] A. Zawadzka, et al., Properties and applications of hybrid organic-inorganic halide perovskites thin films, in: Proceedings Volume 11277, Organic Photonic Materials and Devices XXII, 2020, p. 112770S, https://doi.org/10.1117/12.2545957.
[21] A. Laouid, et al., Generation of red light with intense photoluminescence assisted by Forster resonance energy transfer from Znq_2 and DCM thin films, Environ. Sci. Pollut. Res. 30 (2023) 81647–81666, https://doi.org/10.1007/s11356-022-23217-z.
[22] A. Marjanowska, et al., Perovskite thin films for optoelectronic devices: study of their stability, in: 2023 23rd International Conference on Transparent Optical Networks (ICTON), 2023 23550109, https://doi.org/10.1109/ICTON59386.2023.10207408.
[23] A. Zawadzka, et al., Diagnostic and control of linear and nonlinear optical effects in selected self-assembled metallophthalocyanine chlorides nanostructures, Dyes Pigments 157 (2018) 151–162, https://doi.org/10.1016/j.dyepig.2018.04.048.
[24] M. Lougdali, et al., Linear and nonlinear optical properties of Manganese bis-(8-hydroxyquinoline) thin films for optoelectronic devices: experimental and computational studies, J. Mol. Struct. 1249 (2022) 131558, https://doi.org/10.1016/j.molstruc.2021.131558.
[25] R. Anoua, et al., Optical and electronic properties of the natural Alizarin dye: theoretical and experimental investigations for DSSCs application, Opt. Mater. 127 (2022) 112113, https://doi.org/10.1016/j.optmat.2022.112113.
[26] M. Lougdali, et al., Experimental and computational analysis of the Linear and Nonlinear optical properties of Magnesium bis-(8-hydroxyquinoline) thin film, J. Alloys Compd. 921 (2022) 165947, https://doi.org/10.1016/j.jallcom.2022.165947.
[27] D. Weber, $CH_3NH_3PbX_3$, ein Pb(II)-System mit kubischer Perowskitstruktur/$CH_3NH_3PbX_3$, a Pb(II)-System with Cubic Perovskite Structure, Z. Naturforsch. B Chem. Sci. 33 (1978) 1443–1445, https://doi.org/10.1515/znb-1978-1214.
[28] P.S. Whitfield, et al., Structures, phase transitions and tricritical behavior of the hybrid perovskite methyl ammonium lead iodide, Sci. Rep. 6 (2016) 35685, https://doi.org/10.1038/srep35685.
[29] C. Quarti, et al., Structural and optical properties of methylammonium lead iodide across the tetragonal to cubic phase transition: implications for perovskite solar cells, Energy Environ. Sci. 9 (2016) 1754–5692, https://doi.org/10.1039/C5EE02925B.
[30] F. Brivio, et al., Lattice dynamics and vibrational spectra of the orthorhombic, tetragonal, and cubic phases of methylammonium lead iodide, Phys. Rev. B 92 (2015) 144308. https://link.aps.org/doi/10.1103/PhysRevB.92.144308.
[31] Y. Kawamura, et al., Structural study on cubic–tetragonal transition of $CH_3NH3PbI3$, J. Phys. Soc. Jpn. 71 (2002) 1694–1697, https://doi.org/10.1143/JPSJ.71.1694.
[32] K.P. Ong, et al., Structural evolution in methylammonium lead iodide $CH_3NH3PbI3$, J. Phys. Chem. 119 (2015) 1089–5639, https://doi.org/10.1021/acs.jpca.5b09884.
[33] R. Anoua, et al., Optical and morphological properties of *Curcuma longa* dye for dye-sensitized solar cells, Environ. Sci. Pollut. Res. 28 (2021) 57860–57871, https://doi.org/10.1007/s11356-021-14551-9.
[34] A. Laouid, et al., Optical and morphological properties of DCM thin films co-doped of Znq2 by PVD: theoretical and experimental investigations, Vacuum 222 (2024) 112997, https://doi.org/10.1016/j.vacuum.2024.112997.
[35] electronic source: http://gwyddion.net/documentation/user-guide-en/statistical-analysis.html.
[36] N.A. Torkhov, V.A. Buchelnikova, A.A. Mosunov, et al., AFM methods for studying the morphology and micromechanical properties of the membrane of human buccal epithelium cell, Sci. Rep. 13 (2023) 10917, https://doi.org/10.1038/s41598-023-33881-x.
[37] O.S. Heavens, Optical Properties of Thin Solid Films, Courier Corporation, Toronto, 1991. ISBN 0486669246, 9780486669243.
[38] N. Bouchenak Khelladi, et al., Simulation study of optical transmission properties of ZnO thin film deposited on different substrates, Am. J. Opt. Photon. 1 (2013) 2330–8494, https://doi.org/10.11648/j.ajop.20130101.11.
[39] H.A. Macleod, Thin-Film Optical Filters, fourth ed., CRC Press, 2010 https://doi.org/10.1201/9781420073034. ISBN 9780429136511.
[40] E.G. Birgin, et al., Estimation of the optical constants and the thickness of thin films using unconstrained optimization, J. Comput. Phys. 151 (1999) 862–880, https://doi.org/10.1006/jcph.1999.6224.
[41] A. Marjanowska, et al., Topography and nonlinear optical properties of thin films containing iodide-based hybrid perovskites, Nanomaterials 14 (1) (2024) 50, https://doi.org/10.3390/nano14010050.
[42] A.U. Leguy, et al., Reversible hydration of $CH_3NH_3PbI_3$ in films, single crystals, and solar cells, Chem. Mater. 27 (2015) 3397–3407, https://doi.org/10.1021/acs.chemmater.5b00660.